

1 **Similar millennial climate variability on the**
2 **Iberian margin during two early Pleistocene**
3 **glacials and MIS 3**

B. Birner¹, D. A. Hodell¹, P. C. Tzedakis², L. C. Skinner¹

4 **Key points**

- 5 • Millennial variability was a pervasive feature of early Pleistocene climate
6 • Millennial variability in MIS 38 and 40 resembled Dansgaard-Oeschger cycles of MIS 3
7 • The bipolar see-saw was active during most major stadials in the early Pleistocene

8 **Keywords:** Millennial Variability, Interhemispheric Linkage, Iberian Margin, Early Pleistocene

¹Godwin Laboratory for Palaeoclimate Research, Department of Earth Sciences, University of Cambridge, Cambridge, United Kingdom.

²UCL Department of Geography, University College London, London, United Kingdom.

Corresponding author: B. Birner, Godwin Laboratory for Palaeoclimate Research, Department of Earth Sciences, University of Cambridge, Cambridge, United Kingdom

Now at Scripps Institute of Oceanography, University of California San Diego, La Jolla, California 92037, USA. (bbirner@ucsd.edu)

9 Although millennial-scale climate variability (<10 ka) has been well stud-
10 ied during the last glacial cycles, little is known about this important aspect
11 of climate in the early Pleistocene, prior to the Middle Pleistocene Transi-
12 tion. Here we present an early Pleistocene climate record at centennial res-
13 olution for two representative glacials during the ‘41-ka world’ (Marine Iso-
14 tope Stages (MIS) 37–41, from approx. 1235 to 1320 ka) at IODP Site U1385
15 (the ‘Shackleton Site’) on the southwest Iberian margin. Millennial-scale cli-
16 mate variability was suppressed during interglacial periods (MIS 37, MIS 39
17 and MIS 41) and activated during glacial inceptions when benthic $\delta^{18}\text{O}$ ex-
18 ceeded 3.2‰. Millennial variability during glacials MIS 38 and MIS 40 closely
19 resembled Dansgaard-Oeschger events from the last glacial (MIS 3) in am-
20 plitude, shape and pacing. The phasing of oxygen- and carbon-isotope vari-
21 ability is consistent with an active oceanic thermal bipolar see-saw between
22 the Northern and Southern Hemisphere. Most of the prominent stadials in
23 MIS 38 and MIS 40 were associated with a decrease in benthic carbon-isotopes,
24 indicating concomitant changes in the meridional overturning circulation. A
25 comparison to other North Atlantic records of ice-rafting in MIS 38 and MIS 40
26 suggests that freshwater forcing, as proposed for the late Pleistocene, was
27 involved in triggering or amplifying perturbations of the North Atlantic cir-
28 culation that elicited a bipolar see-saw response. Our findings support sim-
29 ilarities in the operation of the climate system occurring on millennial timescales

³⁰ before and after the Middle Pleistocene Transition despite the increases in
³¹ global ice volume and duration of the glacial cycles.

1. Introduction

Earth's climate system during the Pleistocene alternated between glacial and interglacial conditions upon which millennial-scale variability was frequently superimposed. The nature of suborbital variability has been well documented for the last 800,000 years from Greenland and Antarctic ice cores [*Dansgaard et al.*, 1993; *Jouzel et al.*, 2007; *EPICA Community Members*, 2006; *Johnsen et al.*, 1992; *Oeschger et al.*, 1984] as well as marine sediment records [e.g., *Shackleton et al.*, 2000; *Bond et al.*, 1993; *Bond and Lotti*, 1995; *McManus et al.*, 1999; *Margari et al.*, 2010]; however, little is known about millennial-scale variability under the different climatic boundary conditions of the early Pleistocene (herein informally referring to the period 1-2.58 million years ago) when ice volume was smaller and the duration of glacial cycles shorter than during the late Pleistocene (herein informally defined as the last 1 million years). In the early Pleistocene, glacial-interglacial cycles occurred every 41,000 years (the '41-ka world'), corresponding to the period of the Earth's obliquity cycle, whereas in the late Pleistocene, the glacial-interglacial cycles were quasi-periodic, repeating approximately every 100,000 years (the '100-ka world'). In contrast to the 'sawtooth'-shaped, asymmetric glacial cycles of the 100-ka world, the 41-ka cycles were more symmetric, suggesting that climate variables, ice volume in particular, responded almost linearly to orbital insolation forcing [*Raymo and Nisancioglu*, 2003; *Imbrie et al.*, 1992, 1993; *Maslin and Brierley*, 2015]. However, recent work has questioned the symmetry and simple linearity of glacial cycles in the early Pleistocene climate system [*Ashkenazy and Tziperman*, 2004; *Lourens et al.*, 2010]. The difference in climate response to the same orbital forcing before and after the Middle Pleistocene Transition

53 (MPT, ~ 650 – 1100 ka) has been commonly attributed to the smaller ice volumes (~ 50 m
54 sea-level equivalent (SLE)) in the 41-ka world [*Elderfield et al.*, 2012; *Rohling et al.*, 2014;
55 *Clark et al.*, 2006], but the exact cause remains unknown.

56 Substantial climate variability occurred also on suborbital timescales throughout the
57 Pleistocene and may have affected the pattern of glacial-interglacial cycles [*McManus*
58 *et al.*, 1999; *Raymo et al.*, 1998; *Barker et al.*, 2011; *Jouzel et al.*, 2007; *Denton et al.*,
59 2010]. Our understanding of millennial events is, however, strongly biased by the last
60 several glaciations because evidence of millennial climate variability in the early Pleis-
61 tocene is scarce. *Raymo et al.* [1998] first reported considerable millennial variability in
62 ice-rafted debris (IRD) counts and benthic $\delta^{13}\text{C}$ values for Marine Isotope Stage (MIS) 40
63 and MIS 44 (approx. 1.3 to 1.4 million years ago). Coupled changes of both proxies also
64 suggested a possible link between ice-rafting and perturbations of the Atlantic Merid-
65 ional Overturning Circulation (AMOC) but the resolution of the record was too low to
66 be conclusive. *Mc Intyre et al.* [2001] observed IRD events during 1.75–1.83 Ma that re-
67 curred every ~ 2 – 5 ka comparable to pacing of millennial variability in the late Pleistocene.
68 Heinrich Events, however, have only been identified in late Pleistocene glaciations after
69 640 ka and were presumably absent in the early Pleistocene [*Hodell et al.*, 2008]. Some
70 studies have indicated millennial-scale variability increased across the MPT as ice vol-
71 ume expanded [*Weirauch et al.*, 2008], whereas others have observed persistently strong
72 millennial variability in the early Pleistocene [*Raymo et al.*, 1998; *Tzedakis et al.*, 2015;
73 *Grützner and Higgins*, 2010; *Hodell et al.*, 2008].

74 Because the climate response to the same orbital forcing changed substantially across
75 the MPT (e.g., increasing ice volume and duration of glacial cycles), the 41-ka world
76 provides a natural (historical) experiment to study the nature of millennial variability
77 under different climatic boundary conditions than during the 100-ka world. To improve
78 our understanding of millennial events and their significance for the theory of Pleistocene
79 ice ages, we studied millennial-scale climate variability at Integrated Ocean Drilling Pro-
80 gram (IODP) Site U1385 on the Iberian margin off the Portuguese coast ($\sim 37^\circ\text{N}$, 10°W ,
81 Fig. 2). Two glacial-interglacial cycles (MIS 37–39 and MIS 39–41) were selected during
82 the early Pleistocene because they represent a strong and weak glacial cycle, respectively.
83 The interval is well suited for an assessment of early Pleistocene climate because the 41-
84 ka periodicity characteristic of many early Pleistocene ice age cycles was well established
85 during this interval [*Lisiecki and Raymo*, 2005] and the MPT had not yet begun. The
86 new observations are compared to those of the last glacial cycle from piston cores taken
87 close-by to Site U1385.

1.1. The Iberian Margin

88 The Iberian margin is a prime location to study millennial-scale climate variabil-
89 ity, because during the last glacial cycle the isotope records of planktonic and benthic
90 foraminifera from this region simultaneously recorded rapid climate change expressed in
91 Greenland and Antarctic ice cores, respectively [*Shackleton et al.*, 2000, 2004] (Fig. 1).
92 Local sea surface temperature and hence $\delta^{18}\text{O}$ of planktonic foraminifera are linked to
93 temperature in Greenland by migrations of the Polar Front that reached as far south as
94 39°N during Heinrich events [*Voelker and de Abreu*, 2011]. *Shackleton et al.* [2000] showed

95 that each Dansgaard-Oeschger event coincided with a $\delta^{18}\text{O}$ change of 0.8‰ to 1.2‰ in
96 *Globigerina bulloides* at the Iberian margin. Cooling occurred more gradually than the
97 abrupt terminal warming giving rise to a characteristic ‘sawtooth’ pattern [*Shackleton*
98 *et al.*, 2000] that repeated approximately every 1500 years or multiples thereof [*Schulz*,
99 2002].

100 The $\delta^{18}\text{O}$ changes of benthic foraminifera in the same sediment core closely resemble
101 the Antarctic temperature record [*Shackleton et al.*, 2000, 2004; *Skinner et al.*, 2003;
102 *Margari et al.*, 2010, 2014; *Martrat et al.*, 2007]. The millennial-scale benthic $\delta^{18}\text{O}$ signal
103 in Iberian margin cores was first attributed to reductions in continental ice volume during
104 stadials [*Shackleton et al.*, 2000]. Subsequently however, a significant contribution from
105 local hydrographic reorganizations has also been identified [*Skinner et al.*, 2003, 2007].
106 Benthic $\delta^{18}\text{O}$ values typically decreased gradually by $\sim 0.2\text{--}0.5\text{‰}$ during strong Greenland
107 stadials (e.g., Heinrich stadials) and then increased with the onset of the D-O warm phases
108 (Fig. 1). Thus, the benthic oxygen-isotope record leads the planktonic $\delta^{18}\text{O}$ signal by
109 a few hundred years [*Shackleton et al.*, 2000; *Skinner et al.*, 2003, 2007; *Margari et al.*,
110 2010].

111 Under modern conditions, Site U1385 is bathed by recirculated North East Atlantic
112 Deep Water (NEADW), which consists of a mixture of Labrador Sea Water and Iceland-
113 Scotland Overflow Water [*van Aken*, 2000; *Voelker et al.*, 2015; *Jenkins et al.*, 2015]. It
114 is underlain by Lower Deep Water (LDW), a water mass derived from modified AABW.
115 North East Atlantic Deep Water and its glacial counterpart, Glacial North Atlantic In-
116 termediate Water (GNAIW), have different oxygen- and carbon-isotope signatures than

117 the denser LDW or AABW, despite the attenuation of the Antarctic signature along the
118 flow path. The lower $\delta^{13}\text{C}$ of AABW and LDW is related to a different source signature
119 and the remineralization of $\delta^{13}\text{C}$ -depleted organic matter during northward transport.
120 During the last glacial period, the contribution of southern sourced water to the Iberian
121 margin increased relative to northern sources [Adkins, 2013]. On millennial time scales,
122 the $\delta^{13}\text{C}$ values of epibenthic foraminifera are commonly interpreted to reflect variations
123 in North Atlantic Deep Water formation and the Atlantic Meridional Overturning Cir-
124 culation (AMOC) [Shackleton *et al.*, 2000; Skinner *et al.*, 2007; Margari *et al.*, 2010].
125 Decreases in benthic $\delta^{13}\text{C}$ values (reduced AMOC) were abrupt and approximately syn-
126 chronous with increases in planktonic $\delta^{18}\text{O}$ (i.e. Greenland cooling) suggesting a tight
127 coupling of North Atlantic circulation and climate during the last glacial (Fig. 1).

2. Methods

2.1. IODP Site U1385

128 IODP Expedition 339 (“Mediterranean Outflow”) drilled four holes at Site U1385, the
129 “Shackleton Site”, on the SW Iberian margin off the Portuguese coast ($37^{\circ}34.285'\text{N}$,
130 $10^{\circ}7.562'\text{W}$, water depth = 2578 m) (Fig. 2) [Hodell *et al.*, 2013a]. Site U1385 is located on
131 a structural high, the “Promontorio dos Principes de Avis”, where sedimentation has not
132 been disturbed by turbidity currents [Hodell *et al.*, 2013a]. The recovered sediments were
133 analyzed using core scanning XRF at 1 cm resolution and the four holes were correlated
134 on the basis of Ca/Ti to form a continuous 165-m long composite section [Hodell *et al.*,
135 2015]. Here we studied Sections 1 to 6 in Core 339-U1385D-15H (123.59–135.82 meter
136 below sea floor (mbsf)) and Sections 5 and 6 in Core 339-U1385E-16H (135.24–136.97

137 mbsf). The splice tie point between the cores occurs at 147.32 corrected revised meters
138 composite depth (crmcd) where U1385D-15H-6, 80 cm is tied to U1385E-16H-5, 59 cm,
139 yielding a ~ 8 m long section (140.26–148.88 crmcd) spanning MIS 37–41.

2.2. U1385 Chronostratigraphy

140 *Hodell et al.* [2015] produced various age models for Site U1385 derived by oxygen iso-
141 tope stratigraphy, correlation to other records and orbital tuning. Here, we use a revised
142 version of the ‘tuned age model’ of *Hodell et al.* [2015], developed by correlating sed-
143 iment lightness L^* at Site U1385 to precession (rather than 37°N summer insolation).
144 L^* changed in-phase with local insolation and lagged precession minima by roughly 3 ka
145 based on L^* measurements in the radiometrically dated Core MD99-2334K, located nearby
146 [*Skinner et al.*, 2014; *Hodell et al.*, 2015]. We identified one additional age-depth tie point
147 in MIS 40 as sediment color and precession (but not local summer insolation) show a
148 distinct peak around 1300 ka (Fig. S1). No explicit tuning to other orbital parameters
149 was performed, but a fixed response time to local summer insolation was assumed. *Hodell*
150 *et al.* [2015] justified the validity of the tuning procedure through the amplitude modula-
151 tion of precession in the depth domain and demonstrated the age model’s agreement with
152 the Mediterranean sapropel cyclostratigraphy [*Konijnendijk et al.*, 2014]. Because pre-
153 cession and local summer insolation constitute virtually identical tuning targets (except
154 for one additional tie point), the ‘precession-tuned’ age model is a mere refinement of the
155 ‘insolation-tuned age model’ and is thus supported by the same arguments. Age-depth
156 tie points and sedimentation rates for the study interval are shown in Table 1 and supple-
157 mentary Figure S1. Assuming mean sedimentation rates between 7.5 and 15.5 cm/ka, an

158 average temporal resolution of approximately 65 to 130 years was achieved by sampling
159 every centimeter. This is equivalent to or better than most records of millennial-scale
160 climate change during the late Pleistocene and avoids aliasing of the climate signal.

2.3. Stable Isotope Measurements

161 Twenty specimens of the planktonic foraminifer *Globigerina bulloides* and up to five
162 specimens of the epibenthic species *Cibicidoides wuellerstorfi* were selected for stable
163 isotope analysis at 1 cm intervals from the 250–355 μm and >212 μm size fraction, re-
164 spectively, to match the methodology of previous studies from MIS 3 [e.g., *Shackleton*
165 *et al.*, 2000; *Vautravers and Shackleton*, 2006]. Although seasonal production and ver-
166 tical migration of *G. bulloides* might lead to underestimating the absolute amplitude of
167 millennial-scale temperature variability, this applies equally to the previous studies of
168 MIS 3 and hence does not alter our conclusions. Where no *C. wuellerstorfi* specimens
169 were available, *Cibicidoides mundulus* (= *Cibicidoides kullenbergi*) was analyzed instead.
170 In contrast to the epibenthic foraminifer *C. wuellerstorfi*, *C. mundulus* may also exist as
171 a shallow-infaunal species. Because of the lowering of pore water $\delta^{13}\text{C}$ values by organic
172 matter oxidation below the sediment-water interface, $\delta^{13}\text{C}$ values of *C. mundulus* were
173 disregarded but $\delta^{18}\text{O}$ could be used without a correction factor [e.g., *Hodell et al.*, 2008;
174 *Lourens et al.*, 2010; *Hoogakker et al.*, 2010].

175 Stable isotope measurements of foraminiferal calcite were performed at the Godwin
176 Laboratory for Palaeoclimatic Research, Department of Earth Sciences, University of
177 Cambridge. Specimens of *G. bulloides* were cleaned with a solution of 3% hydrogen
178 peroxide to remove organic contaminants, followed by 10 min ultrasonication in acetone.

179 Benthic specimens were not treated before stable isotope analysis. The tests were crushed,
180 dried overnight at 50°C and then analyzed on a VG SIRA mass spectrometer with an
181 attached Micromass MultiCarb autosampler or, if samples were smaller than 80 µg, on
182 a Thermo Fisher MAT253 mass spectrometer with a Thermo Fisher Kiel device. The
183 foraminiferal calcite was reacted with 100% orthophosphoric acid in evacuated vials at
184 70°C and the resulting CO₂ was analyzed after cryogenic removal of water. A total of
185 1643 samples were measured in dual inlet mode relative to an in-house reference gas. The
186 gas is calibrated to the Vienna Pee Dee Belemnite (VPDB) standard using international
187 standards. Instrument precision of repeated standard measurements was ±0.06‰ (1σ)
188 for δ¹³C and ±0.08‰ (1σ) for δ¹⁸O.

2.4. Mg/Ca Analysis

189 Trace metal analysis was performed at the Godwin Laboratory for Palaeoclimatic Re-
190 search, Department of Earth Sciences, University of Cambridge. Up to twenty specimen
191 of the benthic, infaunal foraminifer *Uvigerina peregrina* were selected from samples at
192 ~5–10 cm intervals near the glacial terminations 37/38 and 39/40, using the size frac-
193 tion >212 µm. The shells were oxidatively cleaned following the scheme by *Barker et al.*
194 [2003] to avoid contamination by clays, organic matter, silicate materials, or other surface
195 coatings. If more than ~240 µg of crushed shell material was available, one third was
196 separated for stable isotopes analysis. Samples were analyzed on a Varian VISTA induc-
197 tively coupled plasma atomic emission spectroscopy instrument following the intensity
198 ratio calibration method of *de Villiers* [2002]. Instrument precision was better than 0.5%
199 for Mg/Ca from repeated measurements of laboratory standards. The error increases to

200 $\sim 4\%$ – 6% for replicates of foraminifera from the same depth. Fe/Ca and Mn/Ca were used
201 to evaluate possible contaminations and show insignificant correlation with Mg/Ca. Deep
202 water temperatures and seawater oxygen isotopic compositions ($\delta^{18}\text{O}_w$) were obtained
203 following the methodology of *Elderfield et al.* [2012]. The benthic foraminifer species
204 *U. peregrina* was chosen for the reconstruction because it is less susceptible to the car-
205 bonate ion effect than epibenthic species [*Elderfield et al.*, 2012]. The infaunal habitat
206 of *Uvigerina* was presumably constantly saturated for CaCO_3 preventing the preferen-
207 tial dissolution of Mg-rich calcite, as proposed initially for the deep infaunal foraminifer
208 *Globobulimina affinis* [*Skinner et al.*, 2003, 2007]. If the number of *U. peregrina* specimens
209 was insufficient for both Mg/Ca and oxygen isotope analysis (23% of all Mg/Ca samples),
210 *U. peregrina* Mg/Ca data were combined with *C. wuellerstorfi* $\delta^{18}\text{O}$ measurements and
211 used in the $\delta^{18}\text{O}_w$ calculations instead. An error propagation for Mg/Ca temperatures
212 and $\delta^{18}\text{O}_w$ is provided in the supplementary material.

3. Results

3.1. The Glacial-Interglacial Cycles of MIS 37–41

213 3.1.1. The Benthic $\delta^{18}\text{O}$ Record

214 In Figure 3, we present oxygen and carbon isotopic records of orbital and millennial-scale
215 climate variability at IODP Site U1385 on the Iberian margin as well as the reconstructed
216 temperature and oxygen isotopic composition of deep water at the study location. Benthic
217 $\delta^{18}\text{O}$ values averaged $\sim 2.8\%$ during MIS 41 and increased gradually into MIS 40. Until the
218 beginning of a gradual deglacial decrease in benthic $\delta^{18}\text{O}$ at ~ 1283 ka, benthic $\delta^{18}\text{O}$ varied
219 between 3.2% and 3.9% during MIS 40. At ~ 1288 ka, benthic $\delta^{18}\text{O}$ decreased rapidly

220 from 3.6‰ to 3.1‰, indicating the beginning of interglacial MIS 39. Benthic $\delta^{18}\text{O}$ values
221 averaged $\sim 4.1‰$ during the peak glacial of MIS 38 (1260 to 1252 ka), which is $> 0.2‰$
222 higher than peak values during MIS 40. The deglaciation of MIS 38 occurred in two
223 phases. It began with a gradual benthic $\delta^{18}\text{O}$ decrease at 1254 ka and, in a second stage,
224 accelerated after 1248 ka yielding a $0.7‰$ larger total benthic $\delta^{18}\text{O}$ range than observed
225 during the deglacial process of MIS 40 ($\sim 1.5‰$ versus $\sim 0.8‰$). The substantially different
226 amplitude of the deglacial change is in equal parts the result of stronger glacial conditions
227 (i.e., higher benthic $\delta^{18}\text{O}$) during MIS 38 and lower mean benthic $\delta^{18}\text{O}$ values during
228 MIS 37 ($2.7‰$) than during the weaker interglacial MIS 39 ($3.0‰$).

229 **3.1.2. The Deep Water Temperature and the Ice Volume Record**

230 A similar amplitude dichotomy is observed in $\delta^{18}\text{O}_w$ but not in deep water tempera-
231 tures (Fig. 3). Mg/Ca paleothermometry of the infaunal benthic foraminifer *U. peregrina*
232 reveals that deep water temperatures were $\sim 0.2^\circ\text{C}$ during both MIS 38 and MIS 40.
233 Interglacial deep water temperatures during MIS 37, MIS 39 and MIS 41 were approx-
234 imately 3.5°C . $\delta^{18}\text{O}_w$ reveals considerable differences between the two glacial cycles but
235 the reconstruction was limited by an analytical uncertainty of $\pm 0.23‰$ SMOW (1σ , see
236 supplementary material). During MIS 39–41, $\delta^{18}\text{O}_w$ varied approximately between $0.7‰$
237 and $0.3‰$ and the transition from MIS 40 to MIS 39 was almost indistinguishable. In con-
238 trast, $\delta^{18}\text{O}_w$ values briefly reached $1.2‰$ in MIS 38 and decreased abruptly to $0.1‰$ during
239 the deglaciation. We did not convert $\delta^{18}\text{O}_w$ values to sea level because the oxygen-isotope
240 compositions of early Pleistocene ice sheets are highly uncertain and because $\delta^{18}\text{O}_w$ on

241 the Iberian Margin can also be affected by local hydrographic effects related to deep-water
242 circulation [Skinner *et al.*, 2003, 2007].

3.2. Millennial-Scale Variability in MIS 37–41

243 3.2.1. Suborbital Variability in Planktonic $\delta^{18}\text{O}$

244 Glacials MIS 38 and MIS 40 were characterized by pervasive millennial-scale variability
245 in the planktonic $\delta^{18}\text{O}$ record but millennial variability was suppressed during interglacials
246 MIS 37, MIS 39 and MIS 41 (Fig. 3). Cold stadial events during both glacials have been
247 numbered to facilitate the description of the results. Stadials are numbered sequentially
248 from youngest to oldest, such that Sx.1 represents the terminal stadial event that occurred
249 just prior to deglaciation during MIS x. Some weaker cold events are indicated by blue
250 arrows in Figure 3. The inception of glacial MIS 40 was marked by the first strong
251 millennial event (S40.9) at 1312 ka after benthic $\delta^{18}\text{O}$ exceeded the threshold of 3.2‰
252 (blue dashed line in Fig. 3). During MIS 40, eight further stadial events (S40.1 to
253 S40.8) were recorded in planktonic $\delta^{18}\text{O}$ which had a mean stadial-interstadial range of
254 $1.0\pm 0.16\text{‰}$. The last stadial event in MIS 40 occurred 6 ka before benthic $\delta^{18}\text{O}$ reached
255 interglacial levels and was followed by a gradual decrease of planktonic $\delta^{18}\text{O}$. During
256 MIS 38, a total of nine millennial events (S38.1–S38.9) with an average amplitude of
257 $1.0\pm 0.16\text{‰}$ were recorded after benthic $\delta^{18}\text{O}$ values again exceeded 3.2‰. In contrast
258 to the smaller deglaciation after MIS 40, the termination of MIS 38 occurred in two
259 large, abrupt steps marked by stadial events S38.3 and S38.1. Planktonic $\delta^{18}\text{O}$ typically
260 decreased very rapidly from stadial to interstadial levels at the end of each cold event but
261 increased more slowly at their onset giving rise to a sawtooth-like pattern.

3.2.2. Suborbital Variability in Benthic $\delta^{18}\text{O}$ and $\delta^{13}\text{C}$

Considerable millennial-scale variability is also evident in the benthic oxygen- and carbon-isotope records of Site U1385 (Fig. 3). Strong systematic decreases in benthic $\delta^{18}\text{O}$ and benthic $\delta^{13}\text{C}$ were associated with most major stadials (i.e., stadials terminated by an abrupt planktonic $\delta^{18}\text{O}$ decrease of $\geq 1.0\text{‰}$) during MIS 38 and 40 (i.e., S38.1, S38.3, S38.4, S38.5, S38.8, S40.4 and S40.6–S40.9 but not S40.1). Benthic $\delta^{18}\text{O}$ typically decreased quickly by 0.2–0.4‰ at either the start or shortly after each of these stadials developed their full strength in planktonic $\delta^{18}\text{O}$ and began to return to stadial conditions when planktonic $\delta^{18}\text{O}$ decreased abruptly. In contrast, benthic $\delta^{13}\text{C}$ generally decreased almost simultaneously with the increase of planktonic $\delta^{18}\text{O}$ during the onset of most strong stadials. Coupled changes in planktonic and benthic proxies were evident during termination 37/38 but were lacking during termination 39/40. Some further benthic $\delta^{13}\text{C}$ variability occurred at 1255 ka and 1258 ka during MIS 38, when benthic $\delta^{13}\text{C}$ values briefly rose to interglacial levels.

3.2.3. The Pacing of Millennial-Scale Variability

Figure 4 shows the spectral properties of the detrended isotope time series (the detrending procedure is detailed in the supplementary material). The REDFIT spectrum [Schulz, 2002] of planktonic $\delta^{18}\text{O}$ for MIS 37–41 (Fig. 4d) reveals that variance is focused primarily at five periods: 1.3 ka, 1.7 ka, 2.6 ka, 3.5 ka and 6.0 ka. The 1.3 ka, 1.7 ka, 2.6 ka and 3.5 ka periodicity are significant at the 95% confidence level, whereas the spectral peak at 6.0 ka is only significant at the 80% confidence level against a red noise background. Correspondingly, Morlet wavelet analysis of MIS 37 to MIS 41 (Fig. 4a–c) detects the

284 highest variance in all three isotope proxies at roughly ~ 1.5 ka and ~ 3.5 ka. However,
285 strong variance in the millennial band is exclusive to glacial periods and damped during
286 interglacials. Variance at ~ 6.5 ka is most prominent during the deglaciation after MIS 38
287 and the glacial inceptions of MIS 38 and MIS 40. The time series analysis results remain
288 fundamentally unchanged when the insolation tuned age model of *Hodell et al.* [2015] is
289 used instead (see supplementary materials).

4. Discussion

4.1. Orbital-scale Variability in MIS 37–41

290 Previous sea level reconstructions indicate that sea level varied between +20 m and
291 -70 m relative to the Holocene during the glacial-interglacial cycles of MIS 37–41 [*Rohling*
292 *et al.*, 2014; *Elderfield et al.*, 2012]. MIS 38 was, however, associated with ~ 10 – 20 m lower
293 sea level than MIS 40 in both referenced sea level reconstructions. The U1385 benthic
294 $\delta^{18}\text{O}$ record is consistent with such intermediate ice volumes during MIS 38 and MIS 40
295 and puts both glacials into the sea level range estimated for MIS 3. Lower benthic $\delta^{18}\text{O}$
296 values and a considerably stronger $\delta^{18}\text{O}_w$ excursion during MIS 38 suggest that MIS 38
297 was a stronger glacial than MIS 40 despite the comparable deep water temperatures during
298 both glacials. The different strength of the two glacial-interglacial cycles could be related
299 to ~ 20 W/m^2 lower 65°N peak summer insolation during MIS 38 and ~ 15 W/m^2 higher
300 insolation forcing during MIS 37 than MIS 41 because of an eccentricity minimum that
301 occurred during MIS 40.

4.2. Comparing Millennial-Scale Variability in the Early Pleistocene and MIS 3

302 The millennial variability in the U1385 isotope record of MIS 38 and MIS 40 closely
303 resembled the Dansgaard-Oeschger (D-O) cycles of MIS 3 in shape, magnitude and fre-
304 quency (Figs. 3 & 5). Prominent millennial events in MIS 38 and 40 were characterized
305 by a sawtooth-like pattern in planktonic $\delta^{18}\text{O}$, similar to the typical shape of D-O events
306 in MIS 3. The mean stadial-interstadial range of $1.0\pm 0.16\text{‰}$ during both MIS 38 and 40
307 was virtually identical to the average range of $1.0\pm 0.12\text{‰}$ recorded during MIS 3 [*Vau-*
308 *travers and Shackleton, 2006*]. Similar suborbital variability during the early Pleistocene
309 and MIS 3 is also evident in the chemical composition of sediments at the Iberian margin
310 [*Hodell et al., 2015*] as detailed in the supplementary material. The pacing of millennial
311 events recognized at Site U1385 compares favorably to the frequencies published for other
312 early Pleistocene records [*Mc Intyre et al., 2001; Raymo et al., 1998; Bailey et al., 2012*].
313 *Raymo et al. [1998]* estimated a recurrence interval of 1–5 ka for millennial events, similar
314 to the 2–5 ka range inferred by *Mc Intyre et al. [2001]*. Both estimates are within the
315 range of periods recognized in the time series analysis of the U1385 record (Fig. 4). Al-
316 though the frequency of sub-Milankovitch climate variability in the Pleistocene has been
317 a matter of much debate, the pacing of events at U1385 is also in good agreement with
318 records from the late Pleistocene that indicated primary recurrence intervals between 1
319 to 2 ka and multiples thereof [*Bond et al., 1993; Schulz, 2002; Vautravers and Shackleton,*
320 *2006; Bond et al., 1997; Dansgaard et al., 1993; Oppo et al., 1998*].

321 *Weirauch et al. [2008]* previously suggested an intensification of millennial variability
322 across the Middle Pleistocene Transition and attributed this change to an increase in mean

323 ice volume from the early to late Pleistocene. Other studies, in contrast, found evidence of
324 persistent millennial-scale variability that was recorded at comparable magnitude in proxy
325 records prior to the MPT in the eastern North Atlantic [*Raymo et al.*, 1998; *Grützner and*
326 *Higgins*, 2010; *Hodell et al.*, 2008]. On the basis of the isotope data from Site U1385, we
327 find no significant increase in the magnitude or frequency of millennial events between
328 MIS 37–41 and MIS 3.

329 *Tzedakis et al.* [2015] suggested that the succession of stadials and interstadials including
330 S38.5 to S38.7 appeared similar to a Late Pleistocene Bond cycle of MIS 3, but without
331 the extreme values associated with Heinrich events. Figure 5 compares the Bond-like cycle
332 from MIS 38 to one example from the last glacial between Heinrich events 5 and 4. A
333 sequence of three stadials that continuously increased in intensity occurred between 1263
334 and 1270 ka. The sequence culminated in one exceptionally long cold event, highlighted
335 in dark gray. The Bond-like cycle is also reflected by strong variance at ~ 7 ka in the
336 planktonic $\delta^{18}\text{O}$ and benthic $\delta^{13}\text{C}$ wavelet plots during that time interval (Fig. 4, b & c).
337 However, identifying further Bond-like cycles in MIS 38 and 40 is ambiguous. Although
338 the lack of additional cycles might be due to the short duration of glacials in the 41-ka
339 world, the occurrence of Bond-like cycles in the early Pleistocene would not necessarily be
340 expected owing to their intrinsic relationship to Heinrich events [*Bond et al.*, 1993] that
341 have not been observed in the early Pleistocene [*Hodell et al.*, 2008].

342 Despite the similarities of millennial variability in the early and late Pleistocene, *Hodell*
343 *et al.* [2008] found no evidence of Heinrich events in the geochemical or physical properties
344 of bulk sediments older than 640 ka at IODP Site U1308. Massive ice-rafting events from

345 the Hudson Strait are indicated in the U1308 record only after prolonged (~ 50 ka) periods
346 of ice growth, which could not be accomplished during the shorter glacials of the 41-ka
347 world [Hodell *et al.*, 2008]. This implies that the dynamics of the Laurentide ice sheet
348 prior to the MPT may have precluded Heinrich-like events but did not affect the processes
349 responsible for Dansgaard-Oeschger-like events, as presumably all circum-North Atlantic
350 ice sheets contributed to ice-rafting in the early Pleistocene [Bailey *et al.*, 2012].

4.3. Climate Thresholds of Millennial-Scale Variability

351 *McManus et al.* [1999] proposed that millennial variability was related to an ice vol-
352 ume threshold, such that when ice sheets exceeded a critical size (i.e., when benthic $\delta^{18}\text{O}$
353 $> 3.5\text{‰}$), the amplitude and frequency of variability in ice-rafting and sea-surface temper-
354 ature proxies increased. However, the physical significance of the 3.5‰ threshold remains
355 uncertain because benthic $\delta^{18}\text{O}$ represents a combined signal of temperature and ice vol-
356 ume. Millennial variability was most prominent in the last glacial cycle during MIS 3
357 when ice volumes reached intermediate levels ($\sim 40\text{--}90$ m sea level equivalent [Rohling
358 *et al.*, 2014; Elderfield *et al.*, 2012]). As peak ice volumes during the early Pleistocene
359 were mostly confined to this ‘millennial window’ [Sima *et al.*, 2004], the pervasive occur-
360 rence of millennial events during the early Pleistocene is perhaps not unexpected. Lower
361 benthic $\delta^{18}\text{O}$ thresholds have been suggested for the early Pleistocene, consistent with
362 equally expansive but thinner ice sheets than those of the late Pleistocene [Raymo *et al.*,
363 1998; *Mc Intyre et al.*, 2001; Bailey *et al.*, 2012]. For example, increased climate variability
364 has been recognized during MIS 40 and MIS 44 when benthic $\delta^{18}\text{O}$ values were between
365 3.3‰ and 3.8‰ [Raymo *et al.*, 1998]. Similarly, *Mc Intyre et al.* [2001] suggested the

366 onset of pronounced millennial climate variability when benthic $\delta^{18}\text{O}$ exceeded 3.3‰ to
367 3.5‰ during the period from 1.75 to 1.83 Ma.

368 In Figure 3, the benthic $\delta^{18}\text{O}$ threshold for the onset of strong millennial variability
369 at the Iberian margin is estimated to be 3.2‰ which was crossed during both glacial
370 inceptions. Millennial-scale variability was suppressed during the interglacials MIS 37,
371 MIS 39 and MIS 41. An upper threshold may occur at 3.8‰, as suggested by the lack
372 of millennial events between stadials S38.4 and S38.3, but is less certain. Some further
373 planktonic $\delta^{18}\text{O}$ excursions were recorded in MIS 37–41 outside the defined thresholds but
374 their amplitude and frequency was considerably reduced (blue arrows in Fig. 3).

375 Threshold behavior appears to be an intrinsic feature of millennial variability through-
376 out the Pleistocene, suggesting the same processes could be responsible for confining the
377 window of climate instability. Presumably, millennial variability was activated when ice
378 sheets became large enough to reach the coast and interact with the ocean but thresholds
379 could also indicate low temperatures that permitted abrupt climate change – for example,
380 by sea ice advance in the Nordic Seas [Li *et al.*, 2005, 2010; *McManus et al.*, 1999].

4.4. The Bipolar See-Saw and Freshwater Forcing in the 41-ka World

381 Methane synchronization of ice core records from Greenland and Antarctica revealed
382 asynchronous temperature changes between the two hemispheres on millennial time scales
383 during the last glacial [e.g., *Blunier and Brook*, 2001; *Blunier et al.*, 1997; *Steig and Alley*,
384 2002; *Blunier et al.*, 1998]. This bipolar see-saw pattern has been explained by variability
385 of the meridional overturning circulation [*Broecker*, 1998; *Stocker and Johnsen*, 2003].
386 When deep water formation in the North Atlantic was weakened, less heat was advected

387 by the surface currents from the tropics to high Northern latitudes and the Iberian margin
388 cooled. At the same time, Antarctica warmed because of the reduced heat transport from
389 south to north across the equator. A sudden resumption of the overturning circulation
390 reversed the trends and quickly warmed the North Atlantic region.

391 At the Iberian margin, these changes were co-registered by different proxies and were
392 reflected in the relative phasing of planktonic and benthic $\delta^{18}\text{O}$ variability [*Shackleton*
393 *et al.*, 2000; *Skinner et al.*, 2003; *Shackleton et al.*, 2004]. *Shackleton et al.* [2000] observed
394 that benthic $\delta^{18}\text{O}$ led planktonic $\delta^{18}\text{O}$ on millennial timescales. Although the reasons
395 for local benthic $\delta^{18}\text{O}$ variability are complex, this has been interpreted to reflect the
396 asymmetry of temperature variability between the Northern and Southern Hemispheres
397 [*Margari et al.*, 2010, 2014; *Martrat et al.*, 2007]. Parallel changes in benthic $\delta^{13}\text{C}$ were
398 found to be broadly anti-phased to planktonic $\delta^{18}\text{O}$, suggesting an association between
399 the surface cooling, interhemispheric heat transport and perturbations of the meridional
400 overturning circulation during the late Pleistocene [*Martrat et al.*, 2007; *Shackleton et al.*,
401 2000; *Skinner et al.*, 2007].

402 The relative phasing of the Site U1385 isotope records suggests an active oceanic bipolar
403 see-saw in the 41-ka world of the early Pleistocene. The most prominent stadials in MIS 38
404 and 40 (i.e., stadials terminated by an abrupt planktonic $\delta^{18}\text{O}$ decrease of $\geq 1.0\text{‰}$ except
405 for S40.1) were associated with simultaneous AMOC anomalies, as indicated by benthic
406 $\delta^{13}\text{C}$ (Figs. 3 & 5). However, mean benthic $\delta^{13}\text{C}$ values were slightly lower during the early
407 Pleistocene than MIS 3, perhaps reflecting a generally weakened overturning circulation
408 during the interval or changes in the biological pump in the source regions of NADW and

409 AABW. As in the last glacial, the decline of planktonic $\delta^{18}\text{O}$ at the end of major stadials
410 was preceded by a decrease in benthic $\delta^{18}\text{O}$. Benthic $\delta^{18}\text{O}$ decreases, however, were slightly
411 smaller but more abrupt than during the last glacial, similar to observations from MIS 6
412 [*Margari et al.*, 2010]. Some less prominent stadials were not associated with noticeable
413 decreases in benthic $\delta^{18}\text{O}$ and $\delta^{13}\text{C}$ at Site U1385. It remains unclear whether potential
414 AMOC perturbations were too small to become apparent in the Iberian margin proxy
415 records, or whether the decoupling of the isotope records reflects the lack of a thermal
416 bipolar see-saw during these events.

417 Cross-correlation of the detrended planktonic and benthic isotope records was performed
418 to quantify their relative phasing and is presented in Figure 7 (for detailed methods see
419 supplementary material). The cross-correlation function of Analyseries [*Paillard et al.*,
420 1996] was used to calculate correlation coefficients and identify the leads and lags between
421 the detrended time series. Figure 7 shows that the cross-correlation of the MIS 37–41
422 isotope time series resembles the results of MIS 3. This method estimates a ~ 0.6 ka
423 lead of benthic $\delta^{18}\text{O}$ over planktonic $\delta^{18}\text{O}$ in the early Pleistocene. Planktonic $\delta^{18}\text{O}$ in
424 turn was approximately anti-phased to benthic $\delta^{13}\text{C}$. A cross-correlation analysis of the
425 early Pleistocene record in the depth domain yields similar lag times (see supplementary
426 material). Thus, the phase relationships between the proxy records support the operation
427 of an oceanic bipolar see-saw, analogous to that observed in the last glacial period, (at
428 least) during major millennial events in the early Pleistocene.

429 The similarity of the shape, pacing, amplitude and relative phasing of millennial vari-
430 ability in surface and deep climate records from MIS 38 and MIS 40 in the early Pleistocene

431 and MIS 3 suggests a common mechanism for millennial-scale variability across the MPT
432 despite the large changes in long-term mean climate state. Once a certain climate thresh-
433 old (coinciding with intermediate ice volumes) was crossed, D-O and possibly Bond-like
434 cycles were initiated during early Pleistocene glacials. In addition, the pattern of millen-
435 nial variability is suggestive of an active bipolar see-saw during strong stadials. Although
436 this parallels observations from the late Pleistocene, the absence of Heinrich events during
437 MIS 38 and MIS 40 [Hodell *et al.*, 2008] reveals substantial differences in the dynamics
438 of the Laurentide ice sheet, suggesting different processes were responsible for Heinrich
439 event-like climate perturbations.

440 Freshwater-induced changes in the strength of the thermohaline circulation (THC) are
441 one of the leading hypotheses to explain abrupt climate change [e.g., Broecker, 1994;
442 Shackleton *et al.*, 2000] but the role of freshwater in triggering stadial events has recently
443 been challenged [Barker *et al.*, 2015]. Freshwater from circum-North Atlantic ice sheets
444 may have disrupted the oceanic density structure and reduced or prevented deep water
445 formation. Consistent with proxy evidence, the climate impacts of AMOC perturbations
446 would be most strongly felt in Greenland and the North Atlantic [e.g., Liu *et al.*, 2009;
447 Vellinga and Wood, 2002; Manabe and Stouffer, 1997; Menviel *et al.*, 2014; Kageyama
448 *et al.*, 2010; Manabe and Stouffer, 1988; Ganopolski and Rahmstorf, 2001].

449 Figure 6 shows that, millennial-scale variability on the Iberian margin can be linked
450 to evidence of ice-rafting at other locations in the North Atlantic. Most of the six IRD
451 peaks at ODP Site 983 during MIS 40 [Raymo *et al.*, 1998] are closely aligned with six
452 major increases in planktonic $\delta^{18}\text{O}$ at the Iberian margin. The IRD proxies, Si/Sr and

453 bulk carbonate $\delta^{18}\text{O}$ from IODP Site U1308 [Hodell *et al.*, 2008] also support a connec-
454 tion of stadial events to ice-rafting. However, not all IRD events found at Site 983 are
455 detected at Site U1308. This probably reflects that IRD from different source regions is
456 captured in the two records. Nevertheless, the correlation of the three records strongly
457 suggests a relationship between ice-surging (IRD, Si/Sr and bulk carbonate $\delta^{18}\text{O}$ peaks),
458 perturbations of the meridional overturning circulation (lower benthic $\delta^{13}\text{C}$) and surface
459 cooling (higher planktonic $\delta^{18}\text{O}$) consistent with freshwater forcing of the thermohaline
460 circulation during MIS 37–41. A similar relationship between ice-rafting and overturning
461 circulation has been reported previously [Raymo *et al.*, 1998; Hodell *et al.*, 2008]. How-
462 ever, it remains uncertain whether the association of ice-rafting and stadials in the early
463 Pleistocene reflects iceberg melting that triggered AMOC anomalies or instead indicates
464 that iceberg melting merely enhanced AMOC perturbations and North Atlantic cooling
465 during already established stadials [Barker *et al.*, 2015].

5. Conclusion

466 Millennial-scale variability in surface temperature (inferred from planktonic $\delta^{18}\text{O}$) on
467 the Iberian Margin was very strong during glacials MIS 38 and MIS 40, demonstrating it
468 was a persistent feature of the early Pleistocene glacial periods when glacial-interglacial
469 cycles were occurring regularly at a period of 41 ka. Millennial-scale variability in the late
470 Pleistocene is best expressed during intermediate ice volume states ($\sim 40\text{--}90$ m sea level
471 equivalent) when benthic $\delta^{18}\text{O}$ values were between 3.5‰ and $\sim 4.5\text{‰}$ [McManus *et al.*,
472 1999]. Considering the climate system spent a great amount of time in this ‘millennial
473 window’ during the early Pleistocene, it is perhaps not unexpected that millennial vari-

474 ability was such a prominent feature of glacial climate in the 41-ka world [*Raymo et al.*,
475 1998; *Mc Intyre et al.*, 2001; *Bailey et al.*, 2012].

476 Millennial variability was suppressed during interglacial periods (MIS 37, MIS 39 and
477 MIS 41) and was activated during glacial inceptions when benthic $\delta^{18}\text{O}$ exceeded 3.2‰.
478 A comparison of planktonic $\delta^{18}\text{O}$ values during glacials MIS 38 and 40 to observations
479 of the last glacial period (MIS 3) reveals a high similarity of millennial-scale climate
480 variability in terms of amplitude, shape and pacing. Benthic and planktonic $\delta^{18}\text{O}$ show an
481 asymmetric relative phasing consistent with the operation of an oceanic thermal bipolar
482 see-saw during most strong stadials in the early Pleistocene, similar to that observed
483 during the last glacial. Many of the prominent stadials in MIS 38 and 40 were associated
484 with perturbations of the meridional overturning circulation, as indicated by low benthic
485 $\delta^{13}\text{C}$ values. Furthermore, most stadials on the Iberian Margin can be correlated with
486 IRD events at high-latitude sites in the North Atlantic, suggesting a role of freshwater
487 forcing in the generation or amplification of millennial-scale variability.

488 Our data provide strong evidence of similar millennial-scale climate cycles during the
489 early Pleistocene and MIS 3. Their great similarity implies that millennial variability
490 may have been driven by a common mechanism before and after the Middle Pleistocene
491 Transition despite the large changes in climatic boundary conditions. However, an unan-
492 swered question is whether millennial-scale variability is merely a symptomatic feature of
493 glacial climate or whether it, alternatively, takes an active role in the inception and/or
494 termination of glacial cycles. Improved understanding of the interaction of millennial- and

495 orbital-scale climate variability will lead to a more complete explanation for the observed
496 patterns of climate change during the Pleistocene Ice Ages.

497 **Acknowledgments.**

498 The data presented in this paper will be archived on the PANGAEA and NOAA Pale-
499 oclimate data systems. This work was made possible by a DAAD scholarship and NERC
500 Grant NE/K005804/1. Linda and Jeannie Booth as well as John Nicolson are thanked
501 for laboratory support. We are grateful for James Rolfe's and Ian Mather's expert sta-
502 ble isotope analyses, Simon Crowhurst's assistance with time series analyses and Mervyn
503 Greaves' insightful comments on Mg/Ca paleothermometry. This manuscript was greatly
504 improved by reviews from Ian Bailey and two anonymous reviewers.

References

- 505 Adkins, J. F. (2013), The role of deep ocean circulation in setting glacial climates,
506 *Paleoceanography*, *28*, 539–561, doi:10.1002/palo.20046.
- 507 Ashkenazy, Y., and E. Tziperman (2004), Are the 41 kyr glacial oscillations a linear
508 response to Milankovitch forcing?, *Quaternary Science Reviews*, *23*(18), 1879–1890,
509 doi:10.1016/j.quascirev.2004.04.008.
- 510 Bailey, I., G. L. Foster, P. A. Wilson, L. Jovane, C. D. Storey, C. N. Trueman, and
511 J. Becker (2012), Flux and provenance of ice-rafted debris in the earliest Pleistocene
512 sub-polar North Atlantic Ocean comparable to the last glacial maximum, *Earth and*
513 *Planetary Science Letters*, *341-344*, 222–233, doi:10.1016/j.epsl.2012.05.034.
- 514 Barker, S., M. Greaves, and H. Elderfield (2003), A study of cleaning procedures used for
515 foraminiferal Mg/Ca paleothermometry, *Geochemistry Geophysics Geosystems*, *4*(9),

- 516 1–20, doi:10.1029/2003GC000559.
- 517 Barker, S., G. Knorr, R. Edwards, and F. Parrenin (2011), 800,000 years of abrupt
518 climate variability, *Science*, *334*, 347–352, doi:10.1126/science.1203580.
- 519 Barker, S., J. Chen, X. Gong, L. Jonkers, G. Knorr, and D. Thornalley (2015), Icebergs
520 not the trigger for North Atlantic cold events, *Nature*, *520*, 333–336, doi:10.1038/
521 nature14330.
- 522 Bazin, L., A. Landais, B. Lemieux-Dudon, H. Toyé Mahamadou Kele, D. Veres, F. Par-
523 renin, P. Martinerie, C. Ritz, E. Capron, V. Lipenkov, M. Loutre, D. Raynaud,
524 B. Vinther, A. Svensson, S. O. Rasmussen, M. Severi, T. Blunier, M. Leuenberger,
525 H. Fischer, V. Masson-Delmotte, J. Chappellaz, and E. W. Wolff (2013), An opti-
526 mized multi-proxy, multi-site Antarctic ice and gas orbital chronology (AICC2012):
527 120800 ka, *Climate of the Past*, *9*, 1715–1731, doi:10.5194/cp-9-1715-2013.
- 528 Blunier, T., and E. J. Brook (2001), Timing of millennial-scale climate change in
529 Antarctica and Greenland during the last glacial period, *Science*, *291*, 109–112, doi:
530 10.1126/science.291.5501.109.
- 531 Blunier, T., J. Schwander, B. Stauffer, T. F. Stocker, A. Dällenbach, A. Indermühle,
532 J. Tschumi, J. Chappellaz, D. Raynaud, and J.-M. Barnola (1997), Timing of
533 the Antarctic Cold Reversal and the atmospheric CO₂ increase with respect to
534 the Younger Dryas event, *Geophysical Research Letters*, *24*(21), 2683–2686, doi:
535 10.1029/97GL02658.
- 536 Blunier, T., J. Chappellaz, J. Schander, A. Dallenbach, B. Stauffer, T. F. Stocker,
537 D. Raynaud, J. Jouzel, H. B. Clausen, C. U. Hammer, and S. J. Johnsen (1998),

- 538 Asynchrony of Antarctic and Greenland climate change during the last glacial period,
539 *Nature*, *394*, 739–743, doi:10.1038/29447.
- 540 Bond, G. C., and R. Lotti (1995), Iceberg discharges into the North Atlantic on
541 millennial time scales during the last glaciation., *Science*, *267*, 1005–1010, doi:
542 10.1126/science.267.5200.1005.
- 543 Bond, G. C., W. S. Broecker, S. Johnsen, J. McManus, L. Babeyrie, J. Jouzel, and
544 G. Bonani (1993), Correlations between climate records from North Atlantic sediments
545 and Greenland ice, *Letters to Nature*, *365*, 143–147, doi:10.1038/365143a0.
- 546 Bond, G. C., W. Showers, M. Cheseby, R. Lotti, P. Almasi, P. DeMenocal, P. Priore,
547 H. Cullen, I. Hajdas, and G. Bonani (1997), A pervasive millennial-scale cycle in
548 North Atlantic Holocene and glacial climates, *Science*, *278*, 1257–1266, doi:10.1126/
549 science.278.5341.1257.
- 550 Broecker, W. S. (1994), Massive iceberg discharges as triggers for global climate change,
551 *Nature*, *372*, 421–424, doi:10.1038/372421a0.
- 552 Broecker, W. S. (1998), Paleocean circulation during the Last Deglaciation: A bipolar
553 seesaw?, *Paleoceanography*, *13*(2), 119–121, doi:10.1029/97PA03707.
- 554 Clark, P. U., D. Archer, D. Pollard, J. D. Blum, J. A. Rial, V. Brovkin, A. C. Mix,
555 N. G. Pisias, and M. Roy (2006), The middle Pleistocene transition: characteristics,
556 mechanisms, and implications for long-term changes in atmospheric pCO₂, *Quaternary*
557 *Science Reviews*, *25*(23–24), 3150–3184, doi:10.1016/j.quascirev.2006.07.008.
- 558 Dansgaard, W., S. J. Johnsen, H. B. Clausen, D. Dahl-Jensen, N. S. Gundestrup, C. U.
559 Hammer, C. S. Hvidberg, J. P. Steffensen, A. E. Sveinbjörnsdottir, J. Jouzel, and

- 560 G. C. Bond (1993), Evidence for general instability of past climate from a 250-kyr
561 ice-core record, *Nature*, *364*, 218–210, doi:10.1038/364218a0.
- 562 de Villiers, S. (2002), An intensity ratio calibration method for the accurate determi-
563 nation of Mg/Ca and Sr/Ca of marine carbonates by ICP-AES, *Geochemistry, Geo-*
564 *physics, Geosystems*, *3*, 1001, doi:10.1029/2001GC000169.
- 565 Denton, G. H., R. F. Anderson, J. R. Toggweiler, R. L. Edwards, J. M. Schaefer, and
566 A. E. Putnam (2010), The last glacial termination, *Science*, *328*, 1652–1656, doi:
567 10.1126/science.1184119.
- 568 Elderfield, H., M. Greaves, S. Barker, I. R. Hall, A. Tripathi, P. Ferretti, S. J. Crowhurst,
569 L. Booth, and C. Daunt (2010), A record of bottom water temperature and sea-
570 water $\delta^{18}\text{O}$ for the Southern Ocean over the past 440 kyr based on Mg/Ca of ben-
571 thic foraminiferal *Uvigerina* spp., *Quaternary Science Reviews*, *29*(1–2), 160–169, doi:
572 10.1016/j.quascirev.2009.07.013.
- 573 Elderfield, H., P. Ferretti, S. J. Crowhurst, I. N. McCave, D. A. Hodell, and A. M.
574 Piotrowski (2012), Evolution of ocean temperature and ice volume through the Mid-
575 Pleistocene climate transition, *Science*, *337*, 704–710, doi:10.1126/science.1221294.
- 576 EPICA Community Members (2006), One-to-one coupling of glacial climate variability
577 in Greenland and Antarctica, *Nature*, *444*, 195–198, doi:10.1038/nature05301.
- 578 Ganopolski, A., and S. Rahmstorf (2001), Rapid changes of glacial climate simulated in
579 a coupled climate model., *Nature*, *409*, 153–158, doi:10.1038/35051500.
- 580 Grützner, J., and S. M. Higgins (2010), Threshold behavior of millennial scale vari-
581 ability in deep water hydrography inferred from a 1.1 Ma long record of sedi-

582 ment provenance at the southern Gardar Drift, *Paleoceanography*, *25*, PA4204, doi:
583 10.1029/2009pa001873.

584 Hodell, D. A., J. E. T. Channell, J. H. Curtis, O. E. Romero, and U. Röhl (2008),
585 Onset of "Hudson Strait" Heinrich events in the eastern North Atlantic at the end
586 of the middle Pleistocene transition (~ 640 ka)?, *Paleoceanography*, *23*, PA4218, doi:
587 10.1029/2008PA001591.

588 Hodell, D. A., L. Lourens, D. V. Stow, J. Hernández-Molina, C. Alvarez Zarikian,
589 and the Shackleton Site Project Members (2013a), The "Shackleton Site" (IODP
590 Site U1385) on the Iberian Margin, *Scientific Drilling*, *16*, 13–19, doi:10.5194/
591 sd-16-13-2013.

592 Hodell, D. A., S. J. Crowhurst, L. Skinner, P. C. Tzedakis, V. Margari, J. E. T. Channell,
593 G. Kamenov, S. Maclachlan, and G. Rothwell (2013b), Response of Iberian Margin
594 sediments to orbital and suborbital forcing over the past 420 ka, *Paleoceanography*, *28*,
595 185–199, doi:10.1002/palo.20017.

596 Hodell, D. A., L. Lourens, S. J. Crowhurst, T. Konijnendijk, R. Tjallingii, F. Jimenez-
597 Espejo, L. C. Skinner, P. C. Tzedakis, and Members of the Shackleton Site Project
598 (2015), A reference time scale for Site U1385 (Shackleton Site) on the Iberian Margin,
599 *Global Planetary Change*, *133*, 49–64, doi:10.1016/j.gloplacha.2015.07.002.

600 Hoogakker, B., H. Elderfield, K. Oliver, and S. Crowhurst (2010), Benthic foraminiferal
601 oxygen isotope offsets over the last glacial-interglacial cycle, *Paleoceanography*,
602 *25*(PA4229), 1–11, doi:10.1029/2009PA001870.

- 603 Imbrie, J., E. A. Boyle, S. C. Clemens, A. Duffy, W. R. Howard, G. Kukla, J. Kutzbach,
604 D. G. Martinson, A. McIntyre, N. G. Pisias, W. L. Prell, M. E. Raytoo, N. J. Shack-
605 leton, and J. R. Toggweiler (1992), On the structure and origin of major glaciation
606 cycles 1. Linear responses to Milankovitch forcing, *Paleoceanography*, *7*(6), 701–738,
607 doi:10.1029/92PA02253.
- 608 Imbrie, J., A. Berger, E. A. Boyle, S. C. Clemens, A. Duffy, W. R. Howard, G. Kukla,
609 J. Kutzbach, D. G. Martinson, A. McIntyre, A. C. Mix, J. J. Morley, L. C. Peterson,
610 N. G. Pisias, W. L. Prell, M. E. Raymo, N. J. Shackleton, and J. R. Toggweiler
611 (1993), On the structure and origin of major glacation cycles 2. The 100,000-year
612 cycle, *Paleoceanography*, *8*(6), 699–735, doi:10.1029/93PA02751.
- 613 Jenkins, W. J., W. M. Smethie Jr., E. A. Boyle, and G. A. Cutter (2015), Water
614 Mass Analysis for the U.S. GEOTRACES (GA03) North Atlantic Sections, *Deep Sea*
615 *Research Part II: Topical Studies in Oceanography*, *116*, 6–20, doi:10.1016/j.dsr2.2014.
616 11.018.
- 617 Johnsen, S. J., H. B. Clausen, W. Dansgaard, K. Fuhrer, N. Gundestrup, C. U.
618 Hammer, P. Iversen, J. Jouzel, B. Stauffer, and J. P. Steffensen (1992), Irregular
619 glacial interstadials recorded in a new Greenland ice core, *Nature*, *359*, 311–313, doi:
620 10.1038/359311a0.
- 621 Jouzel, J., V. Masson-Delmotte, O. Cattani, G. Dreyfus, S. Falourd, G. Hoffmann,
622 B. Minster, J. Nouet, J.-M. Barnola, J. Chappellaz, H. Fischer, J. C. Gallet,
623 S. Johnsen, M. Leuenberger, L. Loulergue, D. Luethi, H. Oerter, F. Parrenin, G. Rais-
624 beck, D. Raynaud, A. Schilt, J. Schwander, E. Selmo, R. Souchez, R. Spahni, B. Stauf-

625 fer, J. P. Steffensen, B. Stenni, T. F. Stocker, J. L. Tison, M. Werner, and E. W. Wolff
626 (2007), Orbital and millennial Antarctic climate variability over the past 800,000
627 years., *Science*, *317*, 793–796, doi:10.1126/science.1141038.

628 Kageyama, M., A. Paul, D. M. Roche, and C. J. Van Meerbeeck (2010), Modelling
629 glacial climatic millennial-scale variability related to changes in the Atlantic merid-
630 ional overturning circulation: A review, *Quaternary Science Reviews*, *29*(21), 2931–
631 2956, doi:10.1016/j.quascirev.2010.05.029.

632 Konijnendijk, T. Y. M., M. Ziegler, and L. J. Lourens (2014), Chronological constraints
633 on Pleistocene sapropel depositions from high-resolution geochemical records of ODP
634 Sites 967 and 968, *Newsletters on Stratigraphy*, *47*(3), 263–282, doi:10.1127/0078-0421/
635 2014/0047.

636 Li, C., D. S. Battisti, D. P. Schrag, and E. Tziperman (2005), Abrupt climate shifts in
637 Greenland due to displacements of the sea ice edge, *Geophysical Research Letters*, *32*,
638 L19702, doi:10.1029/2005GL023492.

639 Li, C., D. S. Battisti, and C. M. Bitz (2010), Can North Atlantic sea ice anomalies
640 account for Dansgaard-Oeschger climate signals?, *Journal of Climate*, *23*, 5457–5475,
641 doi:10.1175/2010JCLI3409.1.

642 Lisiecki, L. E., and M. E. Raymo (2005), A Pliocene-Pleistocene stack of 57 globally
643 distributed benthic $\delta^{18}\text{O}$ records, *Paleoceanography*, *20*(PA1003), 1–17, doi:10.1029/
644 2004PA001071.

645 Liu, Z., B. L. Otto-Bliesner, F. He, E. C. Brady, R. Tomas, P. U. Clark, a. E. Carlson,
646 J. Lynch-Stieglitz, W. B. Curry, E. Brook, D. Erickson, R. Jacob, J. Kutzbach, and

- 647 J. Cheng (2009), Transient simulation of last deglaciation with a new mechanism for
648 Bolling-Allerod warming, *Science*, *325*, 310–314, doi:10.1126/science.1171041.
- 649 Lourens, L. J., J. Becker, R. Bintanja, F. J. Hilgen, E. Tuenter, R. S. W. van de Wal,
650 and M. Ziegler (2010), Linear and non-linear response of late Neogene glacial cycles
651 to obliquity forcing and implications for the Milankovitch theory, *Quaternary Science*
652 *Reviews*, *29*(1–2), 352–365, doi:10.1016/j.quascirev.2009.10.018.
- 653 Manabe, S., and R. J. Stouffer (1988), Two stable equilibria of a coupled ocean-
654 atmosphere model, *Journal of Climate*, *1*, 841–866, doi:10.1175/1520-0442(1988)
655 001<0841:TSEOAC>2.0.CO;2.
- 656 Manabe, S., and R. J. Stouffer (1997), Coupled ocean-atmosphere model response to
657 freshwater input: Comparison to Younger Dryas event, *Paleoceanography*, *12*(2), 321–
658 336, doi:10.1029/97PA01763.
- 659 Margari, V., L. C. Skinner, P. C. Tzedakis, A. Ganopolski, M. J. Vautravers, and N. J.
660 Shackleton (2010), The nature of millennial-scale climate variability during the past
661 two glacial periods, *Nature Geoscience*, p. G35070.1, doi:10.1038/ngeo740.
- 662 Margari, V., L. C. Skinner, D. A. Hodell, B. Martrat, S. Toucanne, J. O. Grimalt, P. L.
663 Gibbard, J. P. Lunkka, and P. C. Tzedakis (2014), Land-ocean changes on orbital
664 and millennial time scales and the penultimate glaciation, *Geology*, *42*(3), 183–186,
665 doi:10.1130/G35070.1.
- 666 Martrat, B., J. O. Grimalt, N. J. Shackleton, L. de Abreu, M. A. Hutterli, and T. F.
667 Stocker (2007), Four climate cycles of recurring deep and surface water destabilizations
668 on the Iberian margin, *Science*, *317*, 502–507, doi:10.1126/science.1139994.

- 669 Maslin, M. a., and C. M. Brierley (2015), The role of orbital forcing in the Early Middle
670 Pleistocene Transition, *Quaternary International*, *659*, 1–9, doi:10.1016/j.quaint.2015.
671 01.047, accepted manuscript, in press.
- 672 Mc Intyre, K., M. L. Delaney, and A. C. Ravelo (2001), Millennial-scale climate change
673 and oceanic processes in the Late Pliocene and Early Pleistocene, *Paleoceanography*,
674 *16*(5), 535–543, doi:10.1029/2000PA000526.
- 675 McManus, J. F., D. W. Oppo, and J. L. Cullen (1999), A 0.5-million-year record of
676 millennial-scale climate variability in the North Atlantic, *Science*, *283*, 971–975, doi:
677 10.1126/science.283.5404.971.
- 678 Menviel, L., A. Timmermann, T. Friedrich, and M. H. England (2014), Hindcasting
679 the continuum of Dansgaard-Oeschger variability: mechanisms, patterns and timing,
680 *Climate of the Past*, *10*, 63–77, doi:10.5194/cp-10-63-2014.
- 681 North Greenland Ice Core Project Members (2004), High-resolution record of Northern
682 Hemisphere climate extending into the last interglacial period., *Nature*, *431*, 147–151,
683 doi:10.1038/nature02805.
- 684 Oeschger, H., J. Beer, U. Siegenthaler, B. Stauffer, W. Dansgaard, and C. Langway
685 (1984), Late glacial climate history from ice cores, in *Climate Processes and Climate*
686 *Sensitivity*, edited by J. E. Hansen and T. Takahashi, pp. 299–306, AGU, Washington,
687 D. C., doi:10.1029/GM029p0299.
- 688 Oppo, D. W., J. F. McManus, and J. L. Cullen (1998), Abrupt climate events 500,000
689 to 340,000 years ago: Evidence from subpolar North Atlantic sediments, *Science*, *279*,
690 1335–1338, doi:10.1126/science.279.5355.1335.

- 691 Paillard, D., L. Labeyrie, and P. Yiou (1996), Macintosh Program performs time-series
692 analysis, *Eos, Trans. AGU*, *77*(39), 379, doi:10.1029/96EO00259.
- 693 Raymo, M., K. Ganley, S. Carter, D. Oppo, and J. McManus (1998), Millennial-scale
694 climate instability during the early Pleistocene epoch, *Nature*, *542*, 699–702, doi:
695 10.1038/33658.
- 696 Raymo, M. E., and K. Nisancioglu (2003), The 41 kyr world: Milankovitch’s other
697 unsolved mystery, *Paleoceanography*, *18*, 1011, doi:10.1029/2002PA000791.
- 698 Rohling, E. J., G. L. Foster, K. M. Grant, G. Marino, A. P. Roberts, M. E. Tamisiea,
699 and F. Williams (2014), Sea-level and deep-sea-temperature variability over the past
700 5.3 million years, *Nature*, *508*, 477–482, doi:10.1038/nature13230.
- 701 Ryan, W. B. F., S. M. Carbotte, J. O. Coplan, S. O’Hara, A. Melkonian, R. Arko, R. A.
702 Weissel, V. Ferrini, A. Goodwillie, F. Nitsche, J. Bonczkowski, and R. Zemsky (2009),
703 Global Multi-Resolution Topography synthesis, *Geochemistry Geophysics Geosystems*,
704 *10*, Q03014, doi:10.1029/2008GC002332.
- 705 Schulz, M. (2002), On the 1470-year pacing of Dansgaard-Oeschger warm events, *Paleo-*
706 *oceanography*, *17*(2), 1–9, doi:10.1029/2000PA000571.
- 707 Schulz, M., and M. Mudelsee (2002), REDFIT: Estimating red-noise spectra directly
708 from unevenly spaced paleoclimatic time series, *Computers and Geosciences*, *28*, 421–
709 426, doi:10.1016/S0098-3004(01)00044-9.
- 710 Shackleton, N. J., M. A. Hall, and E. Vincent (2000), Phase relationships between
711 millennial-scale events 64,000–24,000 years, *Paleoceanography*, *15*(6), 565–569, doi:
712 10.1029/2000PA000513.

- 713 Shackleton, N. J., R. G. Fairbanks, T. Chiu, and F. Parrenin (2004), Absolute calibra-
714 tion of the Greenland time scale: implications for Antarctic time scales and for $\Delta^{14}\text{C}$,
715 *Quaternary Science Reviews*, *23*(14–15), 1513–1522, doi:10.1016/j.quascirev.2004.03.
716 006.
- 717 Sima, A., A. Paul, and M. Schulz (2004), The Younger Dryas - An intrinsic feature of
718 late Pleistocene climate change at millennial timescales, *Earth and Planetary Science*
719 *Letters*, *222*, 741–750, doi:10.1016/j.epsl.2004.03.026.
- 720 Skinner, L. C., N. J. Shackleton, and H. Elderfield (2003), Millennial-scale variability
721 of deep-water temperature and $\delta^{18}\text{O}_{dw}$ indicating deep-water source variations in the
722 Northeast Atlantic, 0-34 cal. ka BP, *Geochemistry Geophysics Geosystems*, *4*(12), 1–17,
723 doi:10.1029/2003GC000585.
- 724 Skinner, L. C., and H. Elderfield (2007), Rapid fluctuations in the deep North Atlantic
725 heat budget during the last glacial period, *Paleoceanography*, *22*, PA1205, doi:10.1029/
726 2006PA001338.
- 727 Skinner, L. C., and N. J. Shackleton (2004), Rapid transient changes in northeast At-
728 lantic deep water ventilation age across Termination I, *Paleoceanography*, *19*, PA2005,
729 doi:10.1029/2003PA000983.
- 730 Skinner, L. C., H. Elderfield, and M. A. Hall (2007), Phasing of millennial climate
731 events and Northeast Atlantic deep-water temperature change since 50 ka BP, in
732 *Ocean Circulation: Mechanisms and Impacts - Past and Future Changes of Meridional*
733 *Overturning, Geophys. Monogr. Ser.*, vol 173, edited by A. Schmittner, J. C. H. Chiang,
734 and S. R. Hemming, pp. 197–208, AGU, Washington, D. C., doi:10.1029/173GM14.

- 735 Skinner, L. C., C. Waelbroeck, A. E. Scrivner, and S. J. Fallon (2014), Radiocarbon
736 evidence for alternating northern and southern sources of ventilation of the deep
737 Atlantic carbon pool during the last deglaciation., *Proceedings of the National Academy
738 of Sciences of the United States of America*, *111*(15), 5480–5484, doi:10.1073/pnas.
739 1400668111.
- 740 Steig, E. J., and R. B. Alley (2002), Phase relationships between Antarctica
741 and Greenland climate records, *Annals of Glaciology*, *35*, 451–456, doi:10.3189/
742 172756402781817211.
- 743 Stocker, T. F., and S. J. Johnsen (2003), A minimum thermodynamic model for the
744 bipolar seesaw, *Paleoceanography*, *18*(4), 1087, doi:10.1029/2003PA000920.
- 745 Torrence, C., and G. P. Compo (1998), A practical guide to wavelet analysis, *Bulletin
746 of the American Meteorological Society*, *79*(1), 61–78, doi:10.1175/1520-0477(1998)
747 079<0061:APGTWA>2.0.CO;2.
- 748 Tzedakis, P. C., V. Margari, and D. Hodell (2015), Coupled oceanland millennial-scale
749 changes 1.26 million years ago, recorded at Site U1385 off Portugal, *Global and Plan-
750 etary Change*, pp. 1–6, doi:10.1016/j.gloplacha.2015.10.008, manuscript in press.
- 751 van Aken, H. M. (2000), The hydrography of the mid-latitude Northeast Atlantic Ocean
752 II: The intermediate water masses, *Deep-Sea Research Part I: Oceanographic Research
753 Papers*, *47*, 789–824, doi:10.1016/S0967-0637(99)00112-0.
- 754 Vautravers, M. J., and N. J. Shackleton (2006), Centennial-scale surface hydrology off
755 Portugal during marine isotope stage 3: Insights from planktonic foraminiferal fauna
756 variability, *Paleoceanography*, *21*, PA3004, doi:10.1029/2005PA001144.

- 757 Vellinga, M., and R. A. Wood (2002), Global climatic impacts of a collapse of the
758 Atlantic thermohaline circulation, *Climatic Change*, *54*, 251–267, doi:10.1023/A:
759 1016168827653.
- 760 Voelker, A. H. L., and L. de Abreu (2011), A Review of Abrupt Climate Change Events
761 in the Northeastern Atlantic Ocean (Iberian Margin): Latitudinal, Longitudinal and
762 Vertical Gradients., in *Abrupt Climate Change: Mechanisms, Patterns, and Impacts*,
763 *Geophys. Monogr. Ser.*, vol 193, edited by H. Rashid, L. Polyak, and E. Mosley-
764 Thompson, pp. 15–37, AGU, Washington, D. C., doi:10.1029/2010GM001021.
- 765 Voelker, A. H. L., A. Colman, G. Olack, J. J. Waniek, and D. Hodell (2015), Oxygen and
766 hydrogen isotope signatures of Northeast Atlantic water masses, *Deep Sea Research*
767 *Part II: Topical Studies in Oceanography*, *116*, 89–106, doi:10.1016/j.dsr2.2014.11.006.
- 768 Weirauch, D., K. Billups, and P. Martin (2008), Evolution of millennial-scale climate
769 variability during the mid-Pleistocene, *Paleoceanography*, *23*, PA3216, doi:10.1029/
770 2007PA001584.

Table 1. Age-Depth Tie Points for the ‘Precession-Tuned’ Age Model

Depth (cmcd)	Precession-Tuned Age (ka)	Sedimentation Rate (cm/ka)
134.58	1184.25	-
140.54	1241.00	10.5
142.03	1260.75	7.5
144.64	1281.00	12.9
146.00	1298.25	7.9
148.48	1314.60	15.2
154.85	1355.70	15.5

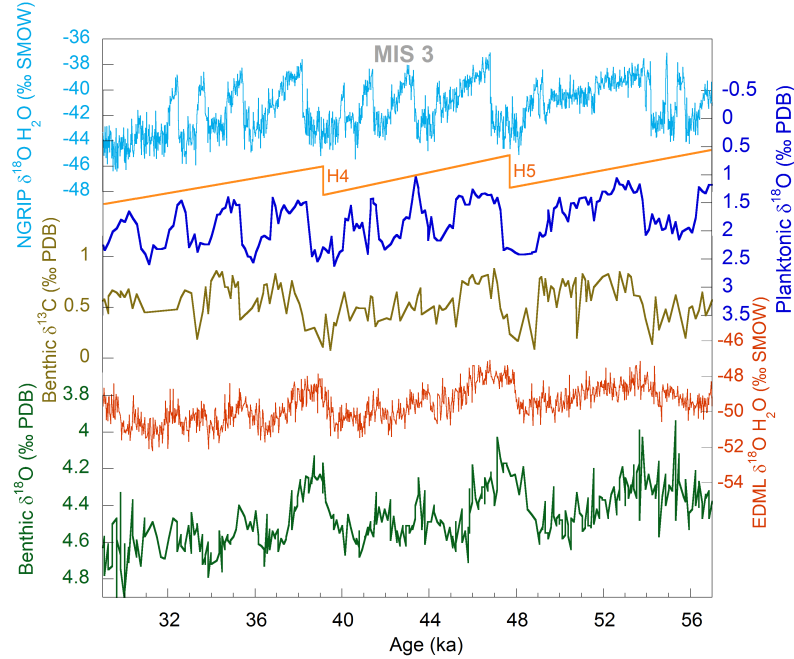


Figure 1. Comparison of planktonic $\delta^{18}\text{O}$ (*G. bulloides*), benthic $\delta^{13}\text{C}$ (*C. Wuellerstorfi*) and benthic $\delta^{18}\text{O}$ (mixed species) from core MD01-2444 [Skinner *et al.*, 2007; Vautravers and Shackleton, 2006] to the NGRIP [North Greenland Ice Core Project Members, 2004] and the EPICA Dronning Maud Land [EPICA Community Members, 2006] $\delta^{18}\text{O}$ records on the AICC2012 synchronized time scale [Bazin *et al.*, 2013]. Orange lines indicate the grouping of D-O events into Bond Cycles [Bond *et al.*, 1997] that are bounded by Heinrich events H3 to H6.

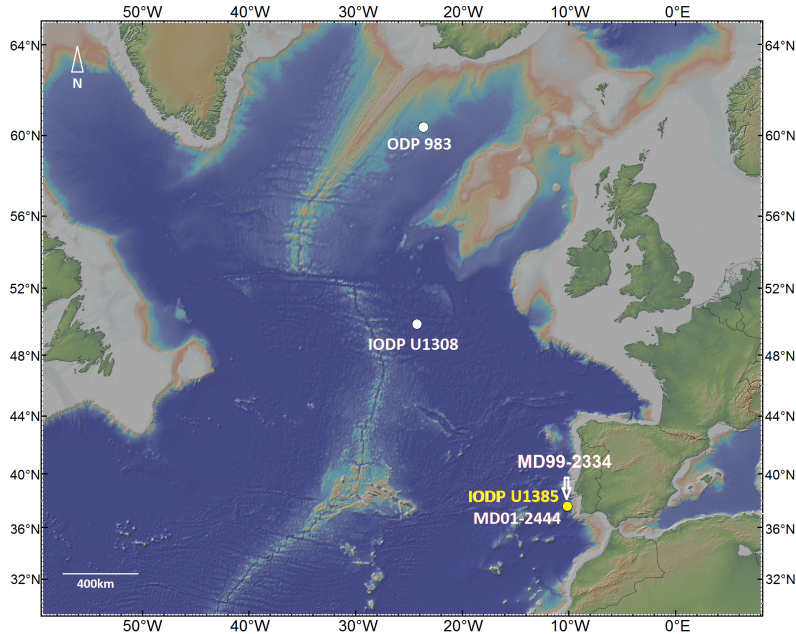


Figure 2. Locations of Integrated Ocean Drilling Program (IODP) sites and piston cores referred to in this study. Site U1385 ($37^{\circ}34.285'N$, $10^{\circ}7.562'W$, water depth = 2578 m) was drilled on the SW Iberian margin at the same location as core MD01-2444. Piston core MD99-2334 ($37^{\circ}48'N$, $10^{\circ}10'W$, water depth = 3246 m) was recovered 26 km to the north. IODP Site U1308 ($49^{\circ}53'N$, $24^{\circ}14'W$, water depth = 3871 m) used by *Hodell et al.* [2008] is a reoccupation of Deep Sea Drilling Project (DSDP) Site 609 and ODP Site 983 ($60^{\circ}24'N$, $23^{\circ}38'W$, water depth = 1983 m) is located on the Garder drift near Iceland [*Raymo et al.*, 1998]. Basemap data are from *Ryan et al.* [2009].

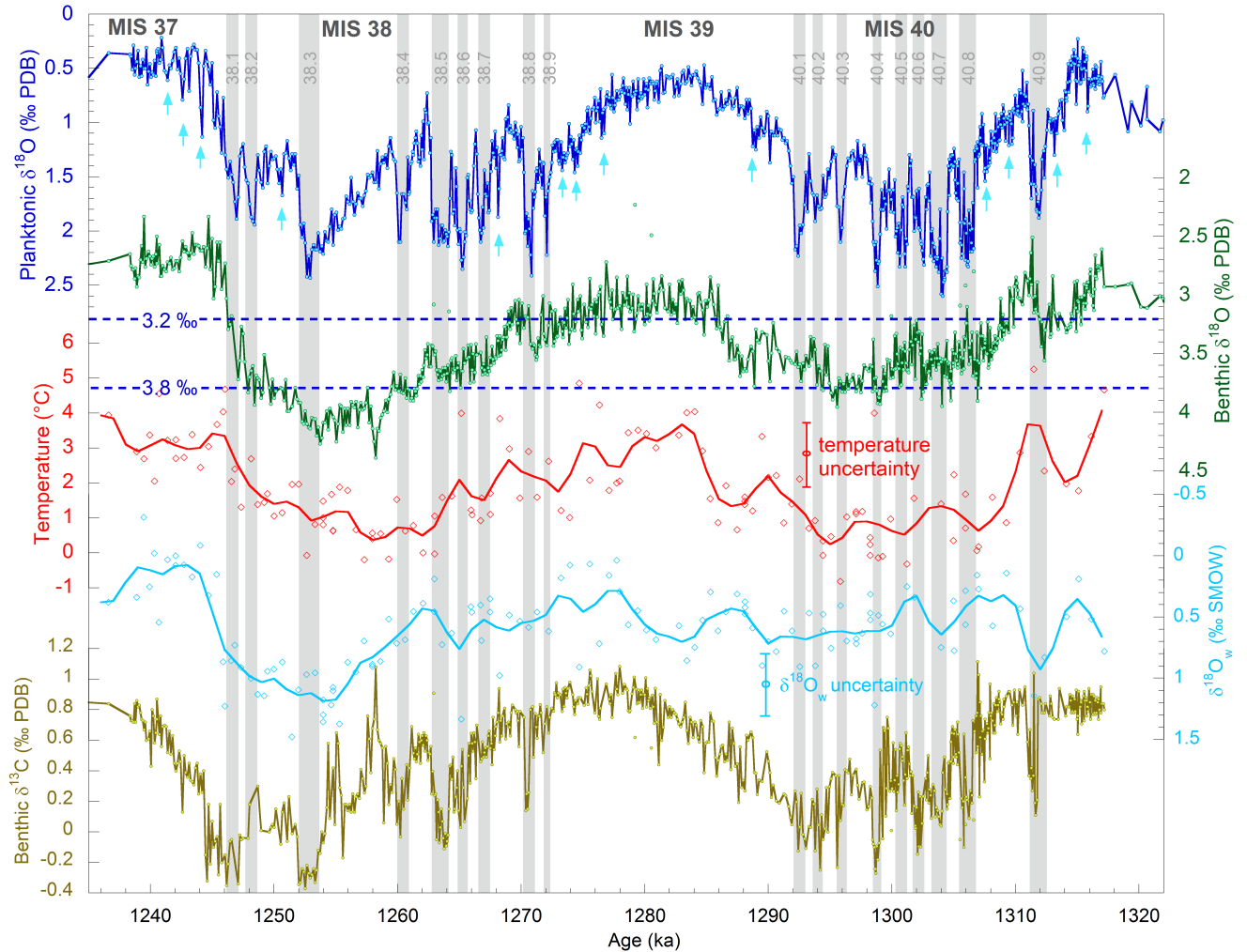


Figure 3. Planktonic $\delta^{18}\text{O}$, benthic $\delta^{18}\text{O}$ and benthic $\delta^{13}\text{C}$ records of millennial-scale variability at Site U1385 on the Iberian margin from Marine Isotope Stages 37 to 41. Mg/Ca temperatures of the infaunal foraminifer *Uvigerina peregrina* are calculated using the core top calibration of *Elderfield et al.* [2010, 2012] and were used to calculate deep water $\delta^{18}\text{O}_w$. The red and light blue curves are smoothed signals (5-ka Gaussian filter) of deep water temperature and $\delta^{18}\text{O}_w$. The error given for both is the propagated standard error $\pm 1\sigma$. The dashed blue lines drawn at 3.2‰ and 3.8‰ represent the oxygen isotope thresholds of climate instability. Gray bars highlight strong millennial-scale cold events and arrows indicate events of smaller amplitude.

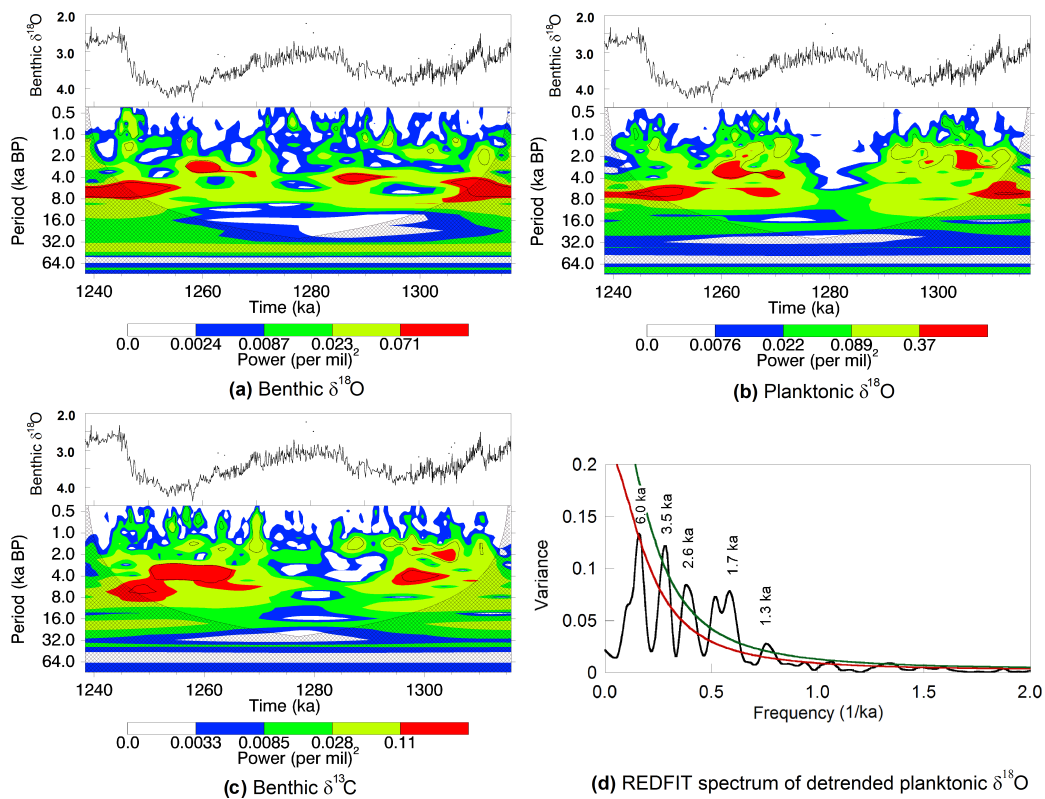


Figure 4. Wavelet analyses of the Site U1385 detrended isotope records including (a) benthic $\delta^{18}\text{O}$, (b) planktonic $\delta^{18}\text{O}$ and (c) benthic $\delta^{13}\text{C}$. Data were detrended by subtracting a 10-ka Gaussian filter from the presmoothed original data (see supplementary material). Wavelet plots (a–c) were created using the data analysis tool at <http://ion.exelisvis.com/> [Torrence and Compo, 1998]. Contour lines give the 95% confidence interval against a red noise background. The hashed area marks the cone of influence where the analysis is affected by edge effects. (d) REDFIT power spectrum [Schulz and Mudelsee, 2002] of planktonic $\delta^{18}\text{O}$ spanning Marine Isotope Stages 37 to 41 (1238.4 to 1317.0 ka). The red and green lines mark the 95% and 80% confidence intervals assuming a red noise model.

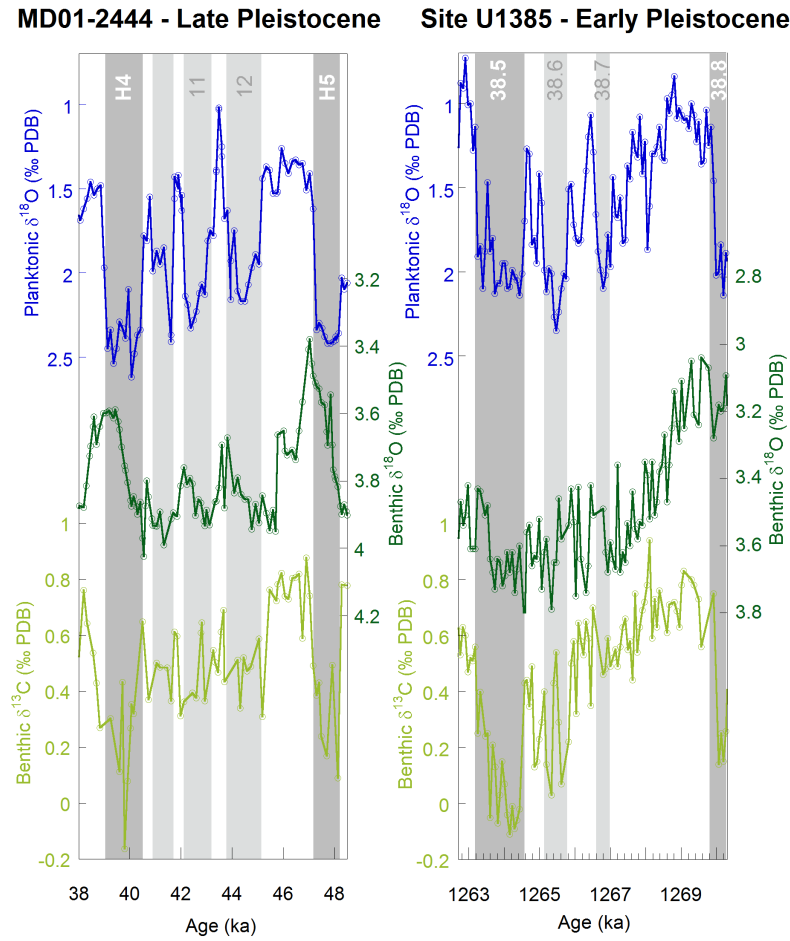


Figure 5. Benthic and planktonic $\delta^{18}\text{O}$ as well as benthic $\delta^{13}\text{C}$ records from the Iberian margin of a potential Bond-like cycle during Marine Isotope Stage (MIS) 38 (right) compared to an example from MIS 3 (left). Light gray bars highlight normal stadials; dark gray shadings indicate the terminal cold events of each Bond-like cycle (Heinrich events in the case of MIS 3). Late Pleistocene data from *Vautravers and Shackleton* [2006], *Skinner et al.* [2007], *Skinner and Elderfield* [2007] and *Skinner* [unpublished] are plotted on the SFP04 age scale of *Shackleton et al.* [2004].

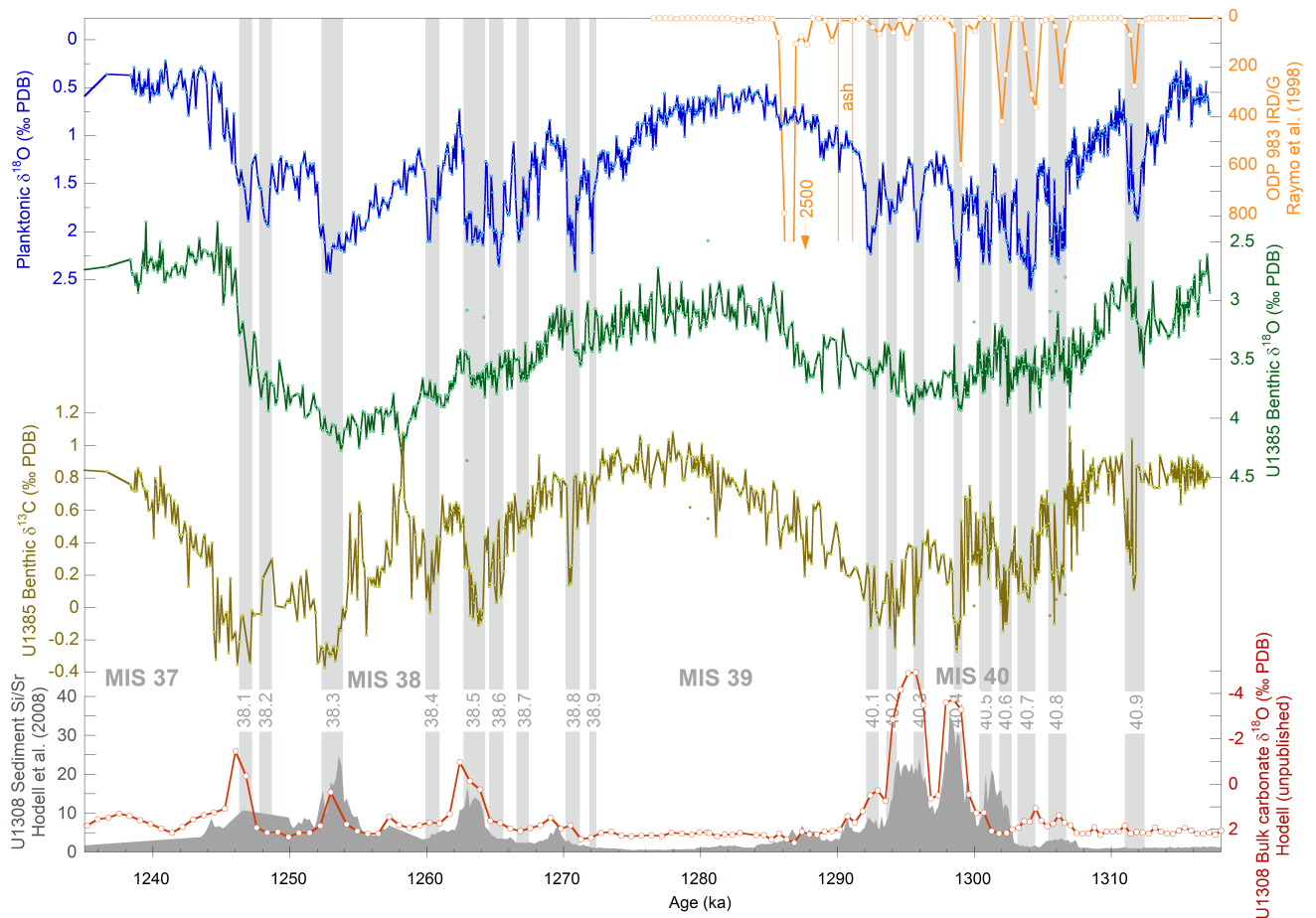


Figure 6. Comparison of the U1385 Iberian margin isotope record with different ice-rafting proxies. The records of Sites ODP 983 [Raymo *et al.*, 1998], IODP U1308 [Hodell *et al.*, 2008] and U1385 have been aligned by correlating their benthic $\delta^{18}\text{O}$ curves (see supplementary material) and are all shown on the precession-tuned age scale of this study. An ash layer is highlighted in the ODP Site 983 record [Raymo *et al.*, 1998]. Sediment Si/Sr and bulk carbonate $\delta^{18}\text{O}$ at IODP Site U1308 have been shown to correlate with IRD input at the site in the late Pleistocene [Hodell *et al.*, 2008].

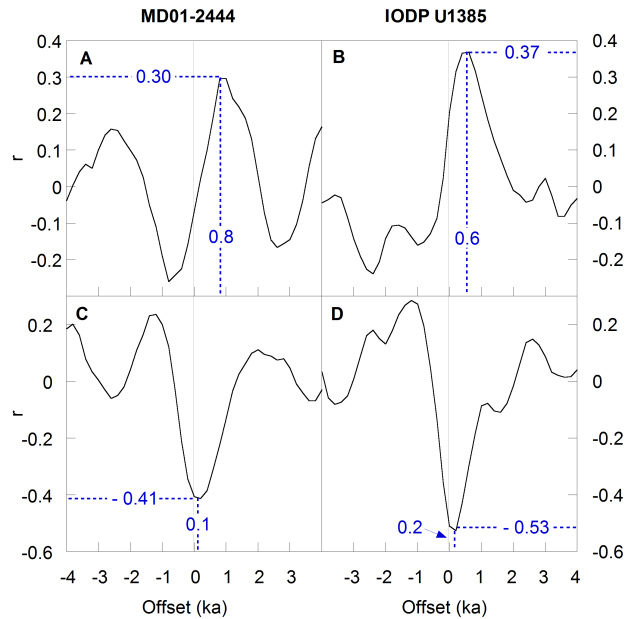


Figure 7. Cross-correlation coefficient (r) of benthic $\delta^{18}\text{O}$ and planktonic $\delta^{18}\text{O}$ for Piston core MD01-2444 (isotope data from *Vautravers and Shackleton* [2006] and *Skinner et al.* [2007] mapped on the Greenland synthetic time-scale of *Barker et al.* [2011] by *Hodell et al.* [2013b]) spanning 10 to 60 ka (A) and U1385 spanning Marine Isotope Stages 37 to 41 (B). (C) and (D) show the cross-correlation coefficient of planktonic $\delta^{18}\text{O}$ and benthic $\delta^{13}\text{C}$ from Site U1385 and MD01-2444 for the same periods. Positive offsets denote a lead of benthic $\delta^{18}\text{O}$ in (A) & (B) or planktonic $\delta^{18}\text{O}$ in (C) & (D), respectively. The smoothed time series were detrended by subtracting a 10-ka trend from the interpolated original data (see supplementary material). The isolated high frequency component was analyzed using the cross-correlation function of *Analyseries* [*Paillard et al.*, 1996].